Talanta 88 (2012) 439–444

Contents lists available at SciVerse ScienceDirect

Talanta

journal homepage: www.elsevier.com/locate/talanta

Fabrication of DNA/graphene/polyaniline nanocomplex for label-free voltammetric detection of DNA hybridization

Meng Du [1], Tao Yang [1], Xiao Li, Kui Jiao *

Shandong Provincial Key Laboratory of Biochemical Analysis, College of Chemistry and Molecular Engineering, Qingdao University of Science and Technology, Qingdao, 266042, China

ARTICLE INFO

Article history:
Received 12 July 2011
Received in revised form 21 October 2011
Accepted 26 October 2011
Available online 9 November 2011

Keywords:
Graphene
Polyaniline
DNA hybridization
Voltammetry
Electrochemical reduction

ABSTRACT

A novel DNA electrochemical biosensor was described for the detection of specific gene sequences. Electrochemically reduced graphene oxide (ERGNO) was prepared on polyaniline (PAN) nanofibers modified glassy carbon electrode (GCE). Compared with the electrochemical reduction of graphene oxide directly on bare GCE (reduction potential: ca. −1.3 V), more positive reduction potential (ca. −1 V) for graphene oxide was observed with the PAN membrane existing. The formed ERGNO/PAN nanocomposites were applied to bind ssDNA probe via the non-covalent assembly. The surface density of ssDNA was calculated by voltammetric studies of redox cations ($[Ru(NH_3)_6]^{3+}$), which were bound to the surface via electrostatic interaction with negative charged phosphate backbone of the DNA. After the hybridization of ssDNA probe with complementary DNA, the response of surface-bound $[Ru(NH_3)_6]^{3+}$ changed obviously, which could been adopted to recognize the DNA hybridization. Under optimal conditions, the dynamic range of the DNA biosensor for detecting the sequence-specific DNA of cauliflower mosaic virus (CaMV35S) gene was from 1.0×10^{-13} to 1.0×10^{-7} mol L^{-1}, with a detection limit of 3.2×10^{-14} mol L^{-1}. This biosensor also showed a high degree of selectivity.

1. Introduction

Due to their principally advantageous properties, carbon materials are being used in a variety of carbon-based electrodes, particularly for electroanalysis and electrosynthesis [1]. The advantageous properties of carbon-based electrodes include wide potential windows, fairly inert electrochemistry, and good electrocatalytic activity for many redox reactions [2]. Graphene, a single layer of carbon, has been touted for its potential as an excellent electrical conductor since its experimental discovery in 2004 [3]. The preparation of high-quality graphene is the first and most crucial step, as the existence of residual defects will heavily impact the electronic properties of graphene. At present, graphene has been prepared by a variety of techniques, mainly including micromechanical cleavage, ultra-high vacuum heat, chemical vapor deposition, epitaxial growth, direct sonication, chemical reduction, and electrochemical reduction [4]. Among these methods, electrochemical reduction method shows promise for the reduction of graphene oxide (GNO) relying on the electrochemical removal of the oxygen functionalities [5].

The interface between nanomaterials and biomolecules is emerging as one of the most diverse and dynamic areas of science and technology. The development of nano/bio interfaces and biocompatible nanomaterials is rapidly growing for optical, mechanical, and electrochemical detection of various biomolecules and cells [6–8]. Graphene is an extraordinarily wonderful material for sensing applications because of its low cost, large surface area, and specific nanosheet structure [9–11]. It is highly expected to couple biomolecules with graphene to develop high-performance sensors for biomolecular recognition. Lu et al. built nanostructures of graphene and DNA [12]. Their tests showed that the fluorescence darkened significantly when ssDNA rested on graphene, but dsDNA only dimmed slightly. Tang et al. found that the fluorescence had been refreshed when adding complementary DNA to ssDNA-graphene structures, suggesting that the hybridized dsDNA left the graphene surface as a new molecule [13]. The fluorescent strategy requires oligonucleotides labeled with fluorophore. The incorporation of a labeling step into nucleic acid assay brings shortcomings, such as limited labeling efficiency, complex multi-step analysis and contamination to samples [14]. So, many attentions have been paid to the development of label-free technologies in the fields of optical and electrochemical DNA biosensors [15].

Label-free electrochemical sensing of DNA hybridization includes indirect and direct measurement methods. Indirect methods are based on the detection of electroactive probe that intercalate or associate with dsDNA [16–18]. Direct methods

* Corresponding author. Tel.: +86 532 84022665; fax: +86 532 84023927.
E-mail address: kjiao@qust.edu.cn (K. Jiao).
[1] These authors contributed equally to this work.

0039-9140/$ – see front matter © 2011 Elsevier B.V. All rights reserved.
doi:10.1016/j.talanta.2011.10.054

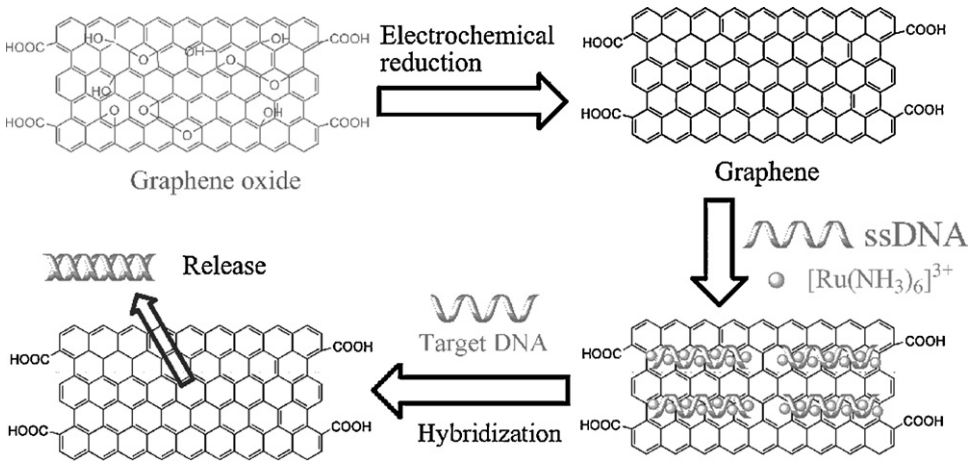

Fig. 1. Schematic illustration of the DNA biosensor.

rely mostly on the intrinsic electroactivity of nucleobases or electroactive functional interfaces [19–21]. However, label-free electrochemical detection of graphene-based DNA hybridization has seldom been reported [22].

In this study, ssDNA/graphene/polyaniline nanocomposites were selected as an electrochemical DNA sensing platform to recognize specific DNA hybridization (Fig. 1). Due to the non-covalent assembly of ERGNO with DNA bases, we anticipated that ERGNO could bind ssDNA probe initially. Subsequently, due to the presence of complementary DNA, the strong and stable binding between ssDNA and complementary DNA would change the conformation of DNA, and weaken the interaction between ssDNA and ERGNO. Such interactions would release ssDNA from the ERGNO surface (partly or totally). The transformation change could be probed by the redox current changes of $[Ru(NH_3)_6]^{3+}$. The experimental results showed that this constructed biosensor was sensitive and selective to the DNA specific sequences of the transgenic genes (the cauliflower mosaic virus 35S (CaMV35S) gene) in the genetically modified crops.

2. Materials and methods

2.1. Apparatus and reagents

A CHI 660C electrochemical analyzer (Shanghai CH Instrument Company, China), which was in connection with a glassy carbon electrode (GCE), a saturated calomel reference electrode (SCE) and a platinum wire counter electrode, was used for the electrochemical measurements. The pH values of all solutions were measured by a model pHS-25 digital acidometer (Shanghai Leici Factory, China). Scanning electron microscopy (SEM) measurements were carried out on a JSM-6700F scanning electron microscope (Japan Electron Company). Sonifier (KQ 100E, 100 W, Kunshan, China).

Polyaniline (PAN) nanofibers were kindly provided by College of Materials Science and Engineering, Qingdao University of Science and Technology [23]. Graphite powder (325 mesh, spectral pure, Sinopharm Chemical Reagent Co., China). Hexaammineruthenium(III) chloride ($[Ru(NH_3)_6]Cl_3$, Alfa Aesar, China). Solutions were all prepared with Aquapro ultrapure water (resistivity: 18 MΩ cm, Aquaplus AWL-1002-P, Ever Young Enterprises Development Co., Ltd., China). The 18-base DNA probe (ssDNA), its complementary DNA (target DNA, namely 18-base fragment of the CaMV35S gene sequence, which is the most frequently used target for genetically modified organism screening in DNA detection [24]), double-base mismatched DNA and noncomplementary DNA (ncDNA) were synthesized by Beijing SBS Gene Tech. Co. Ltd. Their base sequences are listed below:

- ssDNA: 5′-TCT TTG GGA CCA CTG TCG-3′
- target DNA: 5′-CGA CAG TGG TCC CAA AGA-3′
- double-base mismatched DNA: 5′-CGA ***A***AG TGG TCC ***G***AA AGA-3′
- ncDNA: 5′-GCA TCG AGC GAG CAC GTA-3′.

2.2. Fabrication of ssDNA/ERGNO/PAN nanocomposites

Graphite oxide was synthesized from graphite powder by the modified Hummers method as originally presented by Kovtyukhova et al. [25]. In brief, prior to the graphite oxide preparation according to Hummers method [26], an additional graphite oxidation procedure was needed. Graphite was pre-oxidized by concentrated H_2SO_4, $K_2S_2O_8$, and P_2O_5. Then the pre-oxidized graphite was further re-oxidized by concentrated H_2SO_4 and $KMnO_4$. The as-synthesized graphite oxide was suspended in water to obtain a brown dispersion, which was subjected to dialysis for one week to completely remove the residual salts and acids. GNO was obtained by sonicating of the graphite oxide dispersion (0.5 wt%). The obtained brown dispersion was then centrifuged in centrifuge for 5 min at 3000 rpm to remove any unexfoliated graphite oxide.

The GCE (3 mm diameter) was sequentially polished with 0.3 μm and 0.05 μm alumina powder and then washed ultrasonically in water and ethanol for a few minutes, respectively. The cleaned GCE was dried with nitrogen steam for the next modification. The ERGNO/GCE was obtained according to Du et al.'s work [27]. The PAN/GCE was prepared by casting PAN suspension (10 μL) on the GCE surface and dried. GNO suspension (10 μL) was dripped onto the surface of the PAN/GCE and then naturally dried in the air. The GNO film was electrochemically reduced in a phosphate buffer solution (PBS, pH 7.0) for 500 s at −1 V to form ERGNO/PAN/GCE.

The ERGNO/PAN/GCE was immersed in 5 mL Tris-EDTA buffer solution (pH 8.0) containing 1×10^{-6} mol L^{-1} ssDNA at 35 °C for 30 min to bind ssDNA. After that, the ssDNA/ERGNO/PAN/GCE was washed with ultrapure water waiting for hybridization.

2.3. DNA hybridization

DNA hybridization reaction was conducted by dropping 10 μL appropriate concentration of target DNA solution (5 mL Tris-EDTA buffer, pH 8.0) on the ssDNA/ERGNO/PAN recognition surface and keeping reaction for 30 min. Then the electrode was washed with Tris-EDTA buffer. The same procedures as mentioned above were

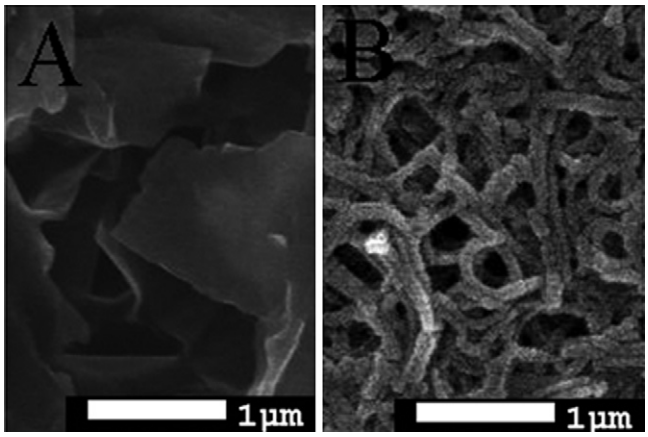

Fig. 2. SEM images of (A) GNO and (B) PAN nanofibers.

applied to the ssDNA/ERGNO/PAN/GCE for the hybridization with double-base mismatched, and ncDNA sequences.

2.4. Electrochemical measurements

The electrochemical performances of the modified electrodes were evaluated by electrochemical impedance spectroscopy (EIS), cyclic voltammetry (CV), and differential pulse voltammetry (DPV). The CV was performed with a scan rate of 100 mV s^{-1}. The EIS was carried out with the AC voltage amplitude of 5 mV, the applied potential of 0.172 V and the voltage frequencies ranged from 10 KHz to 0.01 Hz. The DPV was carried out with the pulse amplitude of 50 mV, the pulse width of 60 ms and the pulse period of 0.2 s. All experiments were conducted at room temperature (25 ± 0.5 °C).

3. Results and discussion

3.1. Characterization

Fig. 2A displayed the SEM image of the synthesized GNO. The typical SEM image of the prepared PAN nanofibers was presented in Fig. 2B. It was found that large quantities of well-defined PAN nanofibers were obtained and they were interconnected together to form netlike nanostructures. The typical length of all the PAN nanofibers was about several micrometers.

Fig. 3A showed CVs of $[Fe(CN)_6]^{3-/4-}$ (1 mmol L^{-1}) on bare GCE, ERGNO/GCE, PAN/GCE, GNO/PAN/GCE, and ERGNO/PAN/GCE. A couple of redox peaks could be observed at bare GCE (a) with the cathodic peak current (I_{pc}) of 2.215×10^{-5} A and the anodic peak current (I_{pa}) of -2.241×10^{-5} A. The current responses ($I_{pc} = 2.676 \times 10^{-5}$ A and $I_{pa} = -2.676 \times 10^{-5}$ A) of ERGNO/GCE (b) increased obviously in comparison with those of GCE, which indicated that the electron transfer rate at ERGNO/GCE was significantly speeded than at GCE. The main reason was attributed to the improved electrical conductivity of ERGNO [27]. For PAN/GCE (c), much larger current responses ($I_{pc} = 3.225 \times 10^{-5}$ A and $I_{pa} = -3.308 \times 10^{-5}$ A) were obtained than at GCE. The large surface area and excellent conductivity of PAN could facilitate the electron transfer of $[Fe(CN)_6]^{3-/4-}$ on the modified electrode [28]. The current responses ($I_{pc} = 1.205 \times 10^{-5}$ A and $I_{pa} = -1.237 \times 10^{-5}$ A) of $[Fe(CN)_6]^{3-/4-}$ at GNO/PAN/GCE decreased compared with that at PAN/GCE, which indicated that the GNO film, being a known insulating layer [29], could lower the electron transfer rate of $[Fe(CN)_6]^{3-/4-}$. After the GNO film was electrochemically reduced, the current responses ($I_{pc} = 3.739 \times 10^{-5}$ A and $I_{pa} = -3.799 \times 10^{-5}$ A) at ERGNO/PAN/GCE (e) were larger than ERGNO/GCE and PAN/GCE. The electroactive surface areas

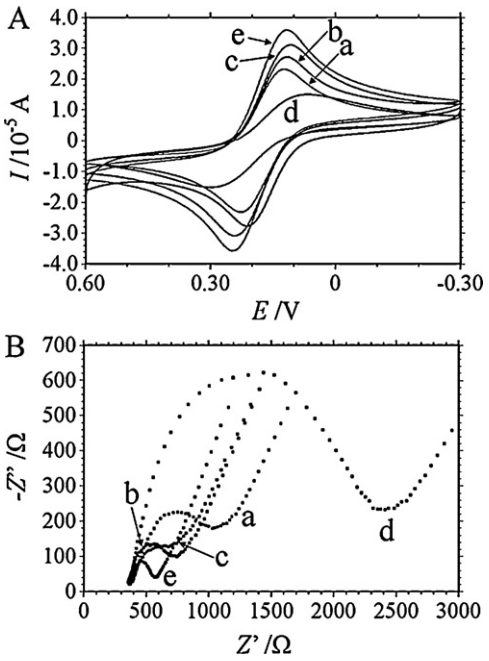

Fig. 3. (A) CVs of 1 mmol L^{-1} $[Fe(CN)_6]^{3-/4-}$ and (B) Nyquist diagrams of 5 mmol L^{-1} $[Fe(CN)_6]^{3-/4-}$ at (a) bare GCE, (b) ERGNO/GCE, (c) PAN/GCE, (d) GNO/PAN/GCE, and (e) ERGNO/PAN/GCE in 0.1 mol L^{-1} KCl.

of the electrodes were estimated according to the slope of I_{pa} versus $v^{1/2}$ plot, based on the Randles-Sevčik equation: $I_{pa} = 2.69 \times 10^5 A D^{1/2} n^{3/2} v^{1/2} C$ [30], where I_{pa} refers to the anodic peak current, n the electron-transfer number, A the surface area of the electrode, D the diffusion coefficient, C the concentration of $[Fe(CN)_6]^{3-/4-}$ and v the scan rate. For $[Fe(CN)_6]^{3-/4-}$ (1 mmol L^{-1}), $n = 1$ and $D = 6.70 \times 10^{-6}$ cm^2 s^{-1}, then from the slope of the I_{pa}–$v^{1/2}$ relation, the active surface areas (average of three measurements) of bare GCE, ERGNO/GCE, PAN/GCE, and ERGNO/PAN/GCE could be calculated to be 0.054, 0.109, 0.125, and 0.148 cm^2, respectively. Herein, the synergistic effect of ERGNO and PAN on enhancing the electroactive surface area was remarkable.

EIS is a useful method for studying the surface properties of the modified electrode [31]. In Nyquist diagram, the semicircle portion observed at high frequencies corresponds to the electron transfer limiting process. The electron transfer resistance, R_{et}, can be directly measured as the semicircle diameter. In Fig. 3B, when ERGNO ($R_{et} = 378\ \Omega$) and PAN ($R_{et} = 346\ \Omega$) was prepared on GCE ($R_{et} = 647\ \Omega$) surface respectively, the semicircle dramatically decreased as compared to bare GCE, suggesting that both ERGNO and PAN promoted the interfacial charge transfer. For GNO/PAN/GCE, the semicircle ($R_{et} = 1980\ \Omega$) dramatically increases as compared to the PAN/GCE, suggesting that GNO acted as an insulating layer which made the interfacial charge transfer difficult and the surface negative charges of GNO (such as carboxyl and hydroxyl) repel the access of $[Fe(CN)_6]^{3-/4-}$ to the electrode surface for electron communication as well. After the GNO film was electrochemically reduced on the electrode, the semicircles of ERGNO/PAN/GCE ($R_{et} = 275\ \Omega$) decrease distinctively. The results were consistent with CVs.

3.2. Electrochemical reduction of GNO on the PAN/GCE

Fig. 4 showed the CVs of GNO/GCE and GNO/PAN/GCE in PBS (0.1 mol L^{-1}, pH 7.0). The GNO/GCE showed a large cathodic current peak at ca. −1.3 V with a starting potential of −0.75 V. This reduction current is the reduction of the oxygen groups of GNO [5]. However, the reduction current disappeared in the second and third

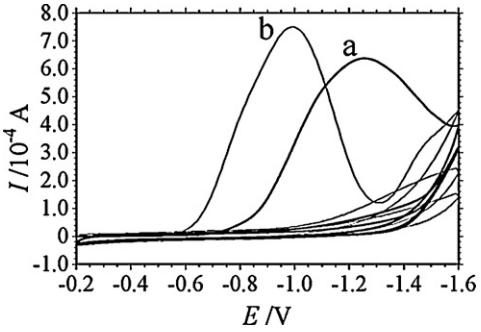

Fig. 4. CVs of (a) GNO/GCE and (b) GNO/PAN/GCE in PBS (pH 7.0) saturated with nitrogen gas.

cycles. This demonstrated that the reduction of surface-oxygenated species at GNO occurred quickly and irreversibly. In comparison, a larger cathodic peak current of GNO/PAN/GCE was observed at ca. −1.0 V. The reduction current also disappeared in the second and third cycles. The results indicated that the PAN film increased the electron transfer rate and shifted the reduction potential of GNO positively.

3.3. Electrochemical characterization of ssDNA/ERGNO/PAN nanocomposites using $[Ru(NH_3)_6]^{3+}$ as a redox marker

$[Ru(NH_3)_6]^{3+}$ was used to study the binding process of ssDNA on ERGNO/PAN/GCE surface. Fig. 5 showed the CV responses of $[Ru(NH_3)_6]^{3+}$ at different electrodes. For ERGNO/PAN/GCE (a), a small redox peak was observed, which was ascribed to the diffusion of $[Ru(NH_3)_6]^{3+}$ to the ERGNO/PAN/GCE. When the ssDNA/ERGNO/PAN/GCE was exposed to a solution containing $[Ru(NH_3)_6]^{3+}$, a pair of larger peaks were observed, showing the electrostatical binding of $[Ru(NH_3)_6]^{3+}$ to ssDNA (b). An obvious difference of the redox potentials between (a) and (b) was observed. The change of the redox potentials could distinguish the background current (caused from the $[Ru(NH_3)_6]^{3+}$ diffusively accessing to the electrode without ssDNA existing) and the current caused from the $[Ru(NH_3)_6]^{3+}$ electrostatically binding to ssDNA. Thus, a high sensitivity can be obtained [32].

The CV measurements allowed a simple calculation for the surface density of ssDNA with the charge integrated from the reduction peak from $[Ru(NH_3)_6]^{3+}$ to $[Ru(NH_3)_6]^{2+}$.

The surface concentration of $[Ru(NH_3)_6]^{3+}$, Γ_{Ru}, could be calculated using Eq. (1):

$$\Gamma_{Ru} = \frac{Q}{nFA} \quad (1)$$

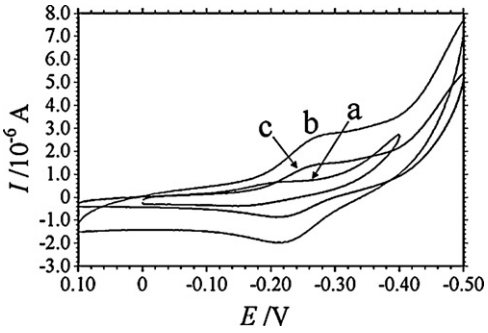

Fig. 5. CVs of 5 μmol L^{-1} $[Ru(NH_3)_6]^{3+}$ recorded at (a) ERGNO/PAN/GCE, (b) ssDNA/ERGNO/PAN/GCE, (c) ssDNA/ERGNO/PAN/GCE hybridized with 1×10^{-7} mol L^{-1} target DNA.

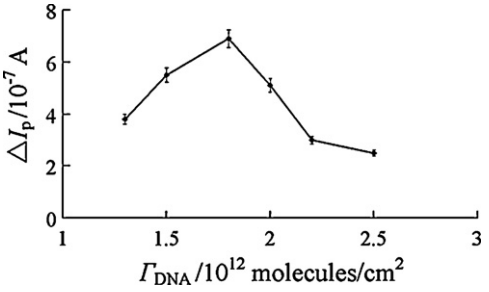

Fig. 6. Influence of the surface density of ssDNA on the sensor signal ΔI_p.

where Q was the charge obtained by integrating the reduction peak area of surface-bound $[Ru(NH_3)_6]^{3+}$, n was the number of electrons involved in the redox reaction, F was Faraday's constant, and A was the electrode area.

Under saturation conditions, the measured value could be converted to the surface density of DNA, Γ_{DNA}, using the following equation:

$$\Gamma_{DNA} = \Gamma_{Ru}\left(\frac{z}{m}\right)N_A \quad (2)$$

where z was the valence of the redox cation, m was the number of nucleotides in the DNA, and N_A was Avogadro's constant. This equation had the same assumptions and conditions as Eq. (1).

Upon incubation with target DNA (1×10^{-7} mol L^{-1}), there was a decrease of $[Ru(NH_3)_6]^{3+}$ due to the release of hybridized dsDNA. It resulted in a substantial decrease of peak current observed by CV measurements (Fig. 5c). The quantity of surface-bound $[Ru(NH_3)_6]^{3+}$ could be determined by integration of the redox peaks, which could be used to determine the surface density of ssDNA on the ERGNO/PAN/GCE surface by Eqs. (1) and (2) [33].

The determination for the surface density of ssDNA was applied to the selection of ssDNA immobilization time. At the same time, DNA hybridization efficiency at electrode surface was sensitively affected on the surface density of ssDNA. A series of ssDNA modified electrodes with different surface densities were prepared by varying immobilization time of ssDNA (1×10^{-6} mol L^{-1}). Fig. 6 showed the correlation between the sensor signal ΔI_p ($\Delta I_p = I_0 - I_{after}$, where I_0 and I_{after} referred to the current obtained before and after ssDNA/ERGNO/PAN/GCE hybridized with target DNA, respectively) and the surface density of ssDNA. It was observed that ΔI_p increased with the increase of surface density originally when the surface density is smaller than 1.8×10^{12} molecules cm^{-2}, then ΔI_p decreased with the further increase of surface density. It ascribed to the hybridization being hindered due to spatial restriction in higher surface density. It clearly indicated that the control of ssDNA immobilization was essential for the sensitivity. The results showed that the ideal surface density was 1.7×10^{12}–1.9×10^{12} molecules cm^{-2}. The immobilization time of 30 min for ssDNA was optimal in the experiments.

3.4. Analytical performance of DNA biosensor

Fig. 7 showed the CVs of $[Ru(NH_3)_6]^{3+}$ at ssDNA/ERGNO/PAN/GCE (a) and at ssDNA/ERGNO/PAN/GCE after it hybridized with the same amount of ncDNA sequence (b), two-base mismatch DNA sequence (c), and target DNA sequence (d). It was clearly observed that a highest signal was observed on ssDNA/ERGNO/PAN/GCE (a). This was because that ssDNA/ERGNO/PAN/GCE presented the most amount of free ssDNA and concomitant negative charges of the electrode surface, which were beneficial to adsorb $[Ru(NH_3)_6]^{3+}$. When ssDNA/ERGNO/PAN/GCE was exposed to ncDNA (b), the peak current and peak type slightly changed compared with

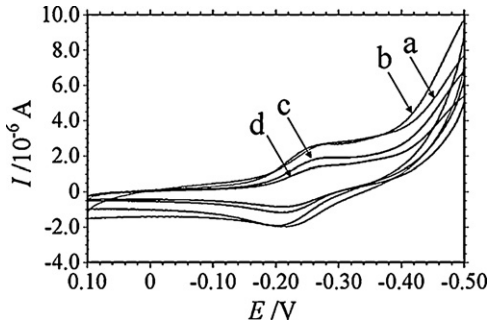

Fig. 7. CVs of 5 μmol L^{-1} $[Ru(NH_3)_6]^{3+}$ recorded at (a) ssDNA/ERGNO/PAN/GCE, (b) ssDNA/ERGNO/PAN/GCE hybridized with ncDNA, (c) the electrode hybridized with double-base mismatched DNA, and (d) the electrode hybridized with target DNA (concentrations of sequence: 1×10^{-7} mol L^{-1}).

curve a, which implied that there was no change occurring at ssDNA/ERGNO/PAN/GCE surface and the hybridization did not happen. For two-base mismatch DNA, the signal was much lower than that of ncDNA sequences (b), but higher than that of target DNA sequences (d), indicating that the hybridization had not been completely accomplished. The result demonstrated that only target DNA sequence could result in a significant decrease of the signal, meaning good selectivity to sequence-specific detection of the sensor.

The sensitivity of the DNA biosensor was investigated by varying the concentration of target DNA. The current responses of $[Ru(NH_3)_6]^{3+}$ (5 μmol L^{-1}) after the sensor hybridized with different concentrations of target DNA were measured by DPV. The average current (I_p) showed a good linear correlation with the concentration of target DNA (C) in the range of 1×10^{-13} to 1×10^{-7} mol L^{-1} (Fig. 8). The regression equation was I_p ($\times 10^{-7}$ A) = $-2.0099 \log C - 10.668$, $R = 0.998$. The detection limit (3σ, where σ was the relative standard deviation (RSD) of the blank solution, $n = 10$) was calculated to be 3.2×10^{-14} mol L^{-1} for target DNA.

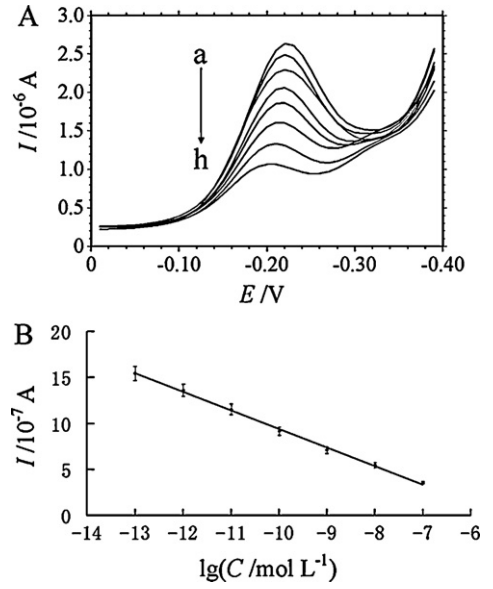

Fig. 8. (A) DPVs of 5 μmol L^{-1} $[Ru(NH_3)_6]^{3+}$ recorded at (a) ssDNA/ERGNO/PAN/GCE, and after hybridization with different concentrations of CaMV35S gene sequence (mol L^{-1}): (b) 1×10^{-13}, (c) 1×10^{-12}, (d) 1×10^{-11}, (e) 1×10^{-10}, (f) 1×10^{-9}, (g) 1×10^{-8}, and (h) 1×10^{-7}. (B) The plot of I_p versus logarithm of target DNA concentration.

Table 1
DPV signals of 5 μmol L^{-1} $[Ru(NH_3)_6]^{3+}$ recorded at ten ssDNA/ERGNO/PAN/GCEs hybridized with 1×10^{-13} mol L^{-1} CaMV35S gene sequence.

Electrode	DPV signal/10^{-7} (A)
1	3.634
2	3.713
3	3.687
4	3.578
5	3.554
6	3.498
7	3.564
8	3.625
9	3.679
10	3.613

3.5. The stability and reproducibility of the DNA biosensor

The ssDNA/ERGNO/PAN/GCE was immersed in B–R buffer (pH 7.0) solution for 60 min. Any decrease of signal was not observed when the electrode was recorded in $[Ru(NH_3)_6]^{3+}$ (5 μmol L^{-1}) after the immersion. The same experiment was conducted by replacing B–R buffer solution with Tris-EDTA buffer (pH 8.0). Also, no signal decrease was observed. Furthermore, the ssDNA/ERGNO/PAN/GCE could be stored at 4 °C for about 2 weeks and the decrease of the signal was gotten as 4.65%. The above results showed that the ssDNA/ERGNO/PAN/GCE was of high stability and could be applied for the hybridization detection. The reproducibility of the DNA biosensor was also investigated. Ten parallel-made ssDNA/ERGNO/PAN/GCEs were used to detect 1×10^{-13} mol L^{-1} target DNA (Table 1). The RSD of the sensor was 5.4% ($n = 10$). It indicated that a satisfactory reproducibility could be obtained by this DNA biosensor.

4. Conclusion

In this study, an efficient DNA hybridization sensing platform based on the ssDNA/ERGNO/PAN nanocomposites was developed. The conductive PAN nanofibers played a significant role in the formation of the nanocomposites. It not only interacted with the basal plane of GNO sheets through π–π stacking, but also promoted the electrochemical reduction of GNO. The DNA hybridization was monitored with label-free voltammetric assay. It was found that the biosensor discriminated mismatched DNA samples of similar lengths. The established DNA biosensor was satisfactorily used for the quantitative detection of CaMV35S gene. This work suggested a simple strategy to prepare a conductive interface for the application in DNA electrochemical biosensing.

Acknowledgements

This project was supported by the National Natural Science Foundation of China (nos. 20805025 and 20975057) and the Natural Science Foundation of Qingdao City (no. 09-1-3-25-ch).

References

[1] D. Kato, N. Sekioka, A. Ueda, R. Kurita, S. Hirono, K. Suzuki, O. Niwa, J. Am. Chem. Soc. 130 (2008) 3716–3717.
[2] R.L. McCreery, Chem. Rev. 108 (2008) 2646–2687.
[3] K.S. Novoselov, A.K. Geim, S.V. Morozov, D. Jiang, Y. Zhang, S.V. Dubonos, I.V. Grigorieva, A.A. Firsov, Science 306 (2004) 666–669.
[4] D.R. Dreyer, S. Park, C.W. Bielawski, R.S. Ruoff, Chem. Soc. Rev. 39 (2010) 228–240.
[5] H.L. Guo, X.F. Wang, Q.Y. Qian, F.B. Wang, X.H. Xia, ACS Nano 3 (2009) 2653–2659.
[6] X. Michalet, F.F. Pinaud, L.A. Bentolila, J.M. Tsay, S. Doose, J.J. Li, G. Sundaresan, A.M. Wu, S.S. Gambhir, S. Weiss, Science 307 (2005) 538–544.
[7] T. Pui, A. Agarwal, F. Ye, N. Balasubramanian, P. Chen, Small 5 (2009) 208–212.
[8] Q. Cao, J.A. Rogers, Adv. Mater. 20 (2008) 29–53.
[9] H.W.C. Postma, Nano Lett. 10 (2010) 420–425.

[10] H.X. Chang, L.H. Tang, Y. Wang, J.H. Jiang, J.H. Li, Anal. Chem. 82 (2010) 2341–2346.
[11] A.K. Geim, Science 324 (2009) 1530–1534.
[12] C.H. Lu, H.H. Yang, C.L. Zhu, G.N. Chen, Angew. Chem. Int. Ed. 48 (2009) 4785–4787.
[13] Z.W. Tang, H. Wu, J.R. Cort, G.W. Buchko, Y.Y. Zhang, Y.Y. Shao, I.A. Aksay, J. Liu, Y.H. Lin, Small 6 (2010) 1205–1209.
[14] C. Batchelor-McAuley, G.G. Wildgoose, R.G. Compton, Biosens. Bioelectron. 24 (2009) 3183–3190.
[15] C.P. Chen, A. Ganguly, C.H. Wang, C.W. Hsu, S. Chattopadhyay, Y.K. Hsu, Y.C. Chang, K.H. Chen, L.C. Chen, Anal. Chem. 81 (2009) 36–42.
[16] E.L.S. Wong, J.J. Gooding, Anal. Chem. 78 (2006) 2138–2144.
[17] F. Ricci, R.Y. Lai, A.J. Heeger, K.W. Plaxco, J.J. Sumner, Langmuir 23 (2007) 6827–6834.
[18] M. Du, T. Yang, Y.C. Zhang, K. Jiao, Electroanalysis 21 (2009) 2521–2526.
[19] X.Z. Zhang, K. Jiao, S.F. Liu, Y.W. Hu, Anal. Chem. 81 (2009) 6006–6012.
[20] W. Zhang, T. Yang, X.M. Zhuang, Z.Y. Guo, K. Jiao, Biosens. Bioelectron. 24 (2009) 2417–2422.
[21] Y.W. Hu, T. Yang, X.X. Wang, K. Jiao, Chem. Eur. J. 16 (2010) 1992–1999.
[22] Y.W. Hu, F.H. Li, X.X. Bai, D. Li, S.C. Hua, K.K. Wang, L. Niu, Chem. Commun. 47 (2011) 1743–1745.
[23] C.Q. Zhang, G.C. Li, H.R. Peng, Mater. Lett. 63 (2009) 592–594.
[24] T.T.N. Lien, T.D. Lam, V.T.H. An, T.V. Hoang, D.T. Quang, D.Q. Khieu, T. Tsukahara, Y.H. Lee, J.S. Kim, Talanta 80 (2010) 1164–1169.
[25] N.I. Kovtyukhova, P.J. Ollivier, B.R. Martin, T.E. Mallouk, S.A. Chizhik, E.V. Buzaneva, A.D. Gorchinskiy, Chem. Mater. 11 (1999) 771–778.
[26] W. Hummers, R. Offeman, J. Am. Chem. Soc. 80 (1958), 1339–1339.
[27] M. Du, T. Yang, K. Jiao, J. Mater. Chem. 20 (2010) 9253–9260.
[28] W. Zhang, T. Yang, X. Li, D.B. Wang, K. Jiao, Biosens. Bioelectron. 25 (2009) 428–434.
[29] C.Z. Zhu, S.J. Guo, Y.X. Fang, S.J. Dong, ACS Nano 4 (2010) 2429–2437.
[30] F. Xiao, F.Q. Zhao, J.W. Li, L.Q. Liu, B.Z. Zeng, Electrochim. Acta 53 (2008) 7781–7788.
[31] I.I. Suni, Trends Anal. Chem. 27 (2008) 604–611.
[32] J. Zhang, J.H. Chen, R.C. Chen, G.N. Chen, F.F. Fu, Biosens. Bioelectron. 25 (2009) 815–819.
[33] A.K.H. Cheng, B.X. Ge, H.Z. Yu, Anal. Chem. 79 (2007) 5158–5164.